RSC Advances

PAPER

View Article Online
View Journal | View Issue

Cite this: *RSC Adv.*, 2017, **7**, 4306

Room temperature synthesis of reduced TiO_2 and its application as a support for catalytic hydrogenation†

Miao Zhang,‡[ab] Qijun Pei,‡[ab] Weidong Chen,[ab] Lin Liu,*[a] Teng He*[a] and Ping Chen[acd]

Received 11th November 2016
Accepted 29th December 2016

DOI: 10.1039/c6ra26667c

www.rsc.org/advances

Reduced TiO_2 (TiO_{2-x}) materials have attracted increasing attention due to their large solar absorption and high photo-activity. However, their synthesis procedures usually involve harsh conditions, such as high temperature and/or high pressure. Herein, a facile solid ball-milling method for the synthesis of TiO_{2-x} under ambient conditions was developed. By using finely dispersed Na/NaCl powders as the reducing agent and TiO_2 (P25, Degussa) as the precursor, a series of TiO_{2-x} of 20–30 nm with a controllable reduction degree can be successfully synthesized through adjusting the reaction conditions. The surface area of TiO_{2-x} is much larger than that of pristine TiO_2, showing its great potential as a catalyst support in chemical reactions. Our experimental results show that uniform Ru particles with particle size less than 1 nm can be well dispersed on the surface of the TiO_{2-x} due to the enhanced surface area and plenty of oxygen vacancies in TiO_{2-x}. As a result, Ru/TiO_{2-x} exhibited superior activity upon catalytic hydrogenation of *N*-methylpyrrole in comparison with Ru/TiO_2.

Introduction

Since Honda and Fujishima discovered hydrogen generation from water by using titanium dioxide (TiO_2) as a photo-electrode,[1] TiO_2 has drawn much attention for its applications in pigments,[2] sunscreens[3] and photocatalysis.[4,5] Apart from the applications in photo-catalysis, TiO_2 is also a unique material widely employed as a catalyst support for selective catalytic hydrogenation,[6–8] oxidation[9,10] and electrochemical[11,12] reactions.

In 2011, Mao *et al.* found that the reduction of TiO_2 nanoparticles through hydrogenation was an effective strategy to improve visible light absorption and photo-activity of TiO_2.[13] Since then, many studies have been devoted to the synthesis of reduced TiO_2 (denoted as TiO_{2-x}) that has abundant oxygen vacancies and Ti^{3+} species. Annealing TiO_2 precursors in a reducing gas atmosphere (H_2 or H_2 plasma) under high temperature and/or high pressure is a common synthetic route for the preparation of TiO_{2-x}.[13,14] Other promising chemical methods including Al vapor,[11] CaH_2 (ref. 15) and $NaBH_4$ (ref. 16) reduction *etc.*, can also produce TiO_{2-x}, where high reaction temperatures were required. Furthermore, electrons, Ar^+ or other high energy particle bombardments have also been employed to produce TiO_{2-x} materials.[17] Despite those significant advances in the synthesis of TiO_{2-x}, it is still highly desirable to develop facile and effective synthetic strategies for the scalable synthesis of TiO_{2-x} under mild conditions.

As a TiO_2 derived material with unique electronic properties, TiO_{2-x} may show promises as a new kind of catalyst support, however, only limited investigations have been published so far. A model study of Au on a reduced titanium oxide ordered film has demonstrated that the strength of the interaction between over-layer Au and the support comprised of strong bonding between Au and Ti, yielding an electron-rich Au and exhibiting an exceptional high activity for CO oxidation.[18] Very recently, the hydrogen treated TiO_2 nanotube arrays with more oxygen vacancies and hydroxyl groups was synthesized which served as highly ordered nanostructured electrode supports and were able to significantly improve the electrochemical performance and durability of fuel cells.[11] The unique properties of the TiO_{2-x} supported catalysts may be derived from (1) the encapsulation of metal particles in TiO_{2-x}, presumably because of the so-called strong metal support interaction (SMSI)[19] between metal and TiO_{2-x}, (2) the strong bonding between the metal atoms at the interface with surface defects (reduced Ti site) or (3) the electrons transfer between metal particles and TiO_{2-x}.[20] It is, therefore, very interesting to investigate the performance of TiO_{2-x} supported catalysts in related chemical reactions.

In this paper, a solid ball-milling reduction process for the synthesis of nanosized TiO_{2-x} from crystalline TiO_2 (P25,

[a]*Dalian National Laboratory for Clean Energy, Dalian Institute of Chemical Physics, Chinese Academy of Sciences, Dalian 116023, China. E-mail: liulin@dicp.ac.cn; heteng@dicp.ac.cn*

[b]*University of the Chinese Academy of Sciences, Beijing 100049, China*

[c]*State Key Laboratory of Catalysis, Dalian Institute of Chemical Physics, Chinese Academy of Sciences, Dalian 116023, China*

[d]*Collaborative Innovation Center of Chemistry for Energy Materials, Dalian 116023, China*

† Electronic supplementary information (ESI) available: More figures of XRD, XPS, TEM, particle size distribution and a table of data. See DOI: 10.1039/c6ra26667c

‡ These authors contributed equally to this study.

Degussa) at room temperature was developed. The reductant is Na that has been well dispersed in NaCl powders. A series of TiO_{2-x} samples with color changing from white to dark blue manifesting the increase in the reduction degree can be facilely prepared. The TiO_{2-x} possesses much higher surface area and visible light absorption than those of the pristine TiO_2. Highly dispersed Ru particles supported on TiO_{2-x} were prepared and tested as catalyst for the hydrogenation of *N*-methylpyrrole, which obviously outperformed that of Ru particles supported on pristine TiO_2, evidencing stronger promoting effect of TiO_{2-x} on Ru.

Experimental section

Chemicals and materials

TiO_2 were purchased from Degussa. Na, $NaBH_4$, NaCl, and NaOH were purchased and used directly without further purification. Tetrahydrofuran (THF) was purchased from Merck, and dried by molecular sieve before usage.

Preparation of Na/NaCl fine powders

Due to the soft and ductile nature of Na metal, NaCl powders were used to disperse Na metal by ball milling.[21] In a typical experiment, Na metal and NaCl powders with a weight ratio of 1/10 were mechanically milled under argon atmosphere using a Retsch PM400 planetary ball milling. All the manipulations were conducted inside a glove box filled with purified argon. The ball milling was carried out at a milling rate of 150 rpm for 4 h at room temperature, and then black Na/NaCl fine powders can be obtained.

Synthesis of TiO_{2-x}

The Na/NaCl fine powder, composed of small Na particles dispersed by NaCl, is expected to be an effective reducing agent for the reduction of crystalline TiO_2 to TiO_{2-x} (Scheme 1). In a typical experiment, crystalline TiO_2 was milled with Na/NaCl fine powders with a weight ratio of $1/n$ (n = 1–4) under argon atmosphere using a Retsch PM400 planetary ball milling, which was carried out at a series of milling rates, such as 80, 120, 150 and 180 rpm at room temperature. The samples milled for 0.25 to 4 hours were collected and washed with deionized water for several times to remove the Na and NaCl. Finally, the obtained TiO_{2-x} products were dispersed in a small amount of deionized water and then vacuum-dried at room temperature to get TiO_{2-x} powders. The synthesized TiO_{2-x} samples are marked as TiO-*n*-*v*-*t*, where n, t and v stand for weight ratio between Na/NaCl and TiO_2, ball milling rate and reaction time, respectively. For example, TiO-4-80-1 means that the obtained TiO_{2-x} was synthesized at a milling rate of 80 rpm for 1 h, and the weight ratio of Na/NaCl fine powders to P25 is 4.

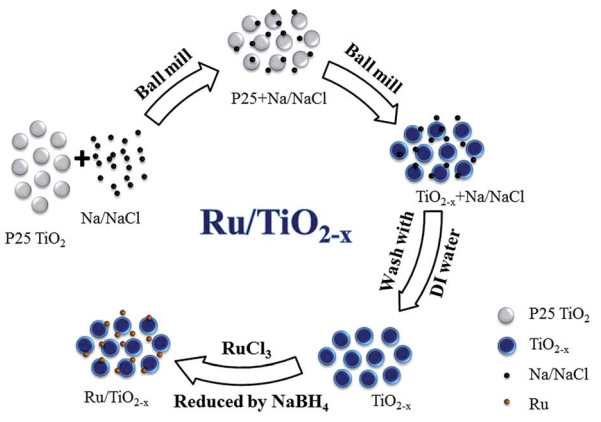

Scheme 1 The route for preparation of Ru/TiO_{2-x}.

Preparations of catalysts and characterizations

5% Ru/TiO_2 and 5% Ru/TiO_{2-x} catalysts were both prepared by a deposition method using $NaBH_4$ as the reducing agent (Scheme 1). The support TiO_2 or TiO_{2-x} was added to a certain concentration of $RuCl_3$ aqueous solutions and stirred for 6 h. Then a $NaBH_4$ solution was added slowly to reduce the Ru^{3+} cations with intensive stirring. Finally the powders were filtered, washed with deionized water and dried under vacuum overnight.

Powder X-ray diffraction (XRD) patterns were recorded on an X'Pert Pro (PANalytical) diffractometer with Cu Kα radiation at 40 kV and 40 mA. Raman spectra were recorded with a Renishaw Raman spectrometer equipped with a He/Ne laser with a wavelength of 514 nm. Transmission electron microscopy (TEM) images were obtained on a JEOL 2000EX electronic microscope operating at 120 kV. High-angle annular dark-field scanning transmission electron microscopy (HAADF-STEM) images were collected on a JEM-2100F instrument equipped with STEM dark-field (DF) detector operating at 200 kV. The specific surface area was measured on Autosorb-1 system (Quantachrome, USA) by N_2 adsorption isotherm through BET method. The X-ray photoelectron spectroscopy (XPS) measurements were performed using an Escalab 250 Xi X-ray photoelectron spectrometer (Thermo Scientific) with non monochromatic Al Kα radiation (photon energy, 1486.6 eV). Due to the overlapped signal of C 1s and Ru 3d, all the samples were mixed with a certain amount of silicon that is used for calibration (Si 2p at 98.4 eV).[22] The UV-Vis absorption spectra were measured on a Shimadzu UV 2600 UV/Vis spectrophotometer. The Ru loadings of the catalysts were determined by inductively coupled plasma spectrometry (ICP-OES, optima 7300DV, Perkin-Elmer, USA).

Hydrogenation of *N*-methylpyrrole

5% Ru/TiO_2 and 5% Ru/TiO_{2-x} catalysts were employed for catalytic hydrogenation of *N*-methylpyrrole (C_5H_7N), which is a commercial chemical with large annual global production. The reactions were carried out in the autoclave reactor (PARR®5500 series compact reactor). 100 mg catalyst (Ru/TiO_2 or Ru/TiO_{2-x}), 425 μL *N*-methylpyrrole and 30 mL THF (as the solvent) were put into the autoclave filled with Ar. The temperature programmer began to heat the reactor with stirring speed of 500 rpm. When the temperature of the reactor was stable at the value we set, 30 atm hydrogen was filled into the

reactor. At this time, the reaction started and the pressure of the reactor was recorded to monitor the hydrogenation progress. The final products were analysed by the gas chromatography (Agilent 7890-B).

Results and discussion

A highly efficient and economic viable reducing agent is needed to synthesize scalable TiO_{2-x} under mild condition. Previous study reported that TiO_2 could be reduced by Al vapor at high temperatures,[23] showing the strong reducing potential of metals. To perform the reduction of TiO_2 at room temperature, a more powerful reductant and a better contact between TiO_2 and reductant are needed. Recently, Na metal dispersed in inert medium (for instance NaCl) has received attention for its use as a very strong reducing agent in the synthesis of NaB_3H_8.[21] The well dispersed Na metal in Na/NaCl may function as a promising reductant for the reduction of TiO_2. Thus, we chose a commercially available crystalline TiO_2 (P25, Degussa), consisting of mixed phases of anatase and rutile, as precursor for the synthesis of TiO_{2-x}. Ball milling of P25 with Na/NaCl fine powders at room temperature and different mechano-chemical conditions led to reduction of P25 into TiO_{2-x} of different oxygen vacancies content as evidenced by the visible color changes after reduction reaction (Fig. 1). The degree of reduction can be facilely controlled by varying the reaction conditions, *i.e.*, weight ratio of P25 nanocrystals to Na/NaCl fine powders, milling rate and reaction time. The synthesized TiO_{2-x} samples are marked as TiO-*n*-*v*-*t*, where *n*, *t* and *v* stand for weight ratio between Na/NaCl and TiO_2, ball milling rate and reaction time, respectively. The color of post-reduced P25 samples ranges from white to light blue and finally to dark blue with the increase of ball milling speed, reaction time and weight ratio of Na/NaCl and P25 (Scheme 1). The corresponding UV-Vis diffuse reflectance spectra clearly show the intensity of the absorption in the visible light region (400–800 nm) gradually increases with the increases of reduction degree, which is consistent with the color changes of the TiO_{2-x} samples (Fig. S1†).

TEM images (Fig. 2) were collected to show the morphology and particle size of the P25 and TiO-4-180-4. The particle size of TiO-4-180-4 sample is similar to that of P25 nanocrystals (20–30 nm), which indicates that such a solid reduction treatment has little influence on the particle size of the reduced TiO_2 samples. Different from that of the pristine P25, disordered layer can be observed on the surface of TiO-4-180-4 particles, which is probably resulted from ball-milling treatment and/or surface reaction between TiO_2 and Na. As a consequence, a remarkable increase of BET surface area was obtained, *i.e.*, the TiO-4-180-4 (113 $m^2\ g^{-1}$) has a BET surface area that is *ca.* 2.5 times of the pristine P25 (45 $m^2\ g^{-1}$).

The crystal structure of TiO_{2-x} is characterized by XRD and compared with that of P25 nanocrystals. As shown in Fig. S2,† a mild reduction treatment with ball milling speed of 80 rpm has little influence on the crystallinity of TiO_{2-x}. However, obvious changes occurred under harsh solid ball milling conditions (longer ball milling time with high Na/TiO_2 ratio or at a high ball milling speed, Fig. 3). Compared with that of the pristine TiO_2, there is no obvious change in the intensities of diffraction peaks corresponding to the rutile phase in the TiO_{2-x} samples treated with different ball milling speeds. However, the intensities of peaks corresponding to the anatase phase significantly weaken with the increase of ball milling speed. The maintenance of rutile phase in the synthesized TiO_{2-x} may be due to its chemical stability compared with that of anatase.

As shown in Fig. 4, P25 nanocrystals display the typical anatase Raman active modes with frequencies at 144, 197, 399, 515, 519 (superimposed with the 515 cm^{-1} band), and 639 cm^{-1} together with modes at 447 and 612 (should peak) cm^{-1} corresponding to the rutile phase.[24] The relatively low intensity of rutile mode may originate from the low Raman response and low content of rutile in the P25.[25] For TiO_{2-x} samples, intensities of peaks corresponding to the rutile phase did not show any obvious change. However, intensities of the peaks corresponding to the anatase phase decreased obviously (Fig. 4e). More

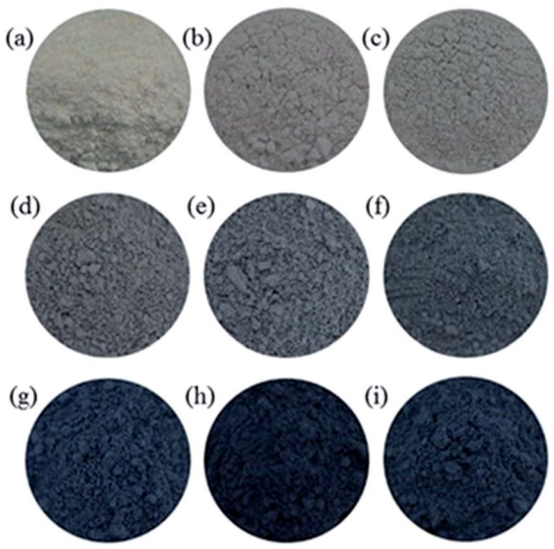

Fig. 1 Photographs of P25 nanocrystals and TiO_{2-x}. (a) P25 nanocrystals; (b) TiO-1-80-0.5; (c) TiO-1-80-1; (d) TiO-1-120-4; (e) TiO-1-150-4; (f) TiO-1-180-4; (g) TiO-2-180-4; (h) TiO-3-180-4 and (i) TiO-4-180-4.

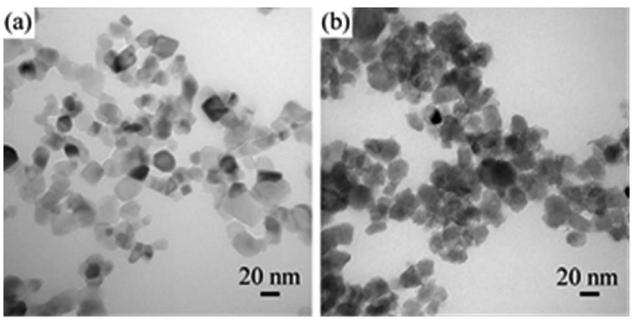

Fig. 2 TEM images of (a) P25 nanocrystals and (b) TiO-4-180-4.

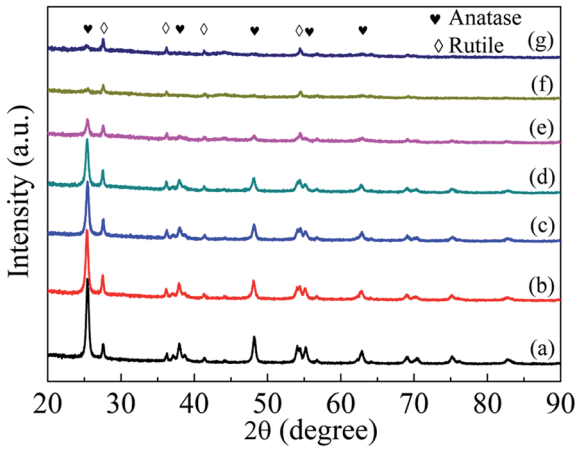

Fig. 3 XRD patterns of P25 nanocrystals and TiO_{2-x} (a) P25 nanocrystals; (b) TiO-1-120-4; (c) TiO-1-150-4; (d) TiO-1-180-4; (e) TiO-2-180-4; (f) TiO-3-180-4 and (g) TiO-4-180-4.

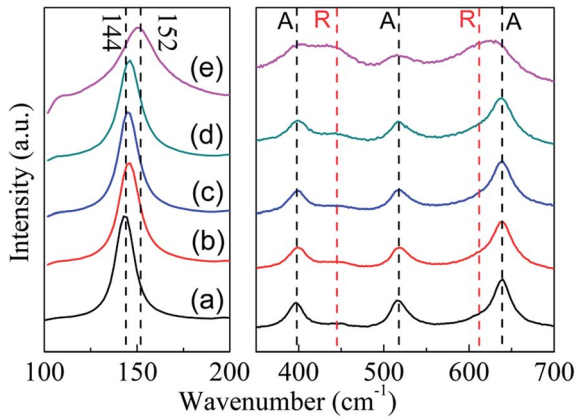

Fig. 4 Raman spectra of P25 nanocrystals and TiO_{2-x} (a) P25 nanocrystals; (b) TiO-1-120-4; (c) TiO-1-150-4; (d) TiO-1-180-4; (e) TiO-4-180-4. A: anatase, R: rutile.

importantly, a blue shift of the strongest E_g mode at 144 cm^{-1} for anatase can be detected. As reported in previous research, this peak shift was mainly caused by the stoichiometry defects in TiO_2.[26] Therefore, the shift in the present study suggests the formation of oxygen vacancies in TiO_{2-x} during solid reduction treatment. Since the anatase was detected by Raman technique, the disappearance of anatase phase in XRD should be attributed to its amorphous state. Noting that the reduction of TiO_2 could mainly occur on its surface or near surface, the synthesized TiO_{2-x} here may have a core–shell structure with reduced shell and unchanged core, which is similar to the results reported in literature.[13]

XPS was also applied to characterize the chemical state of surface elements in TiO-4-180-4. The full XPS survey (Fig. S3†) reveals that no elements other than C, O, Ti can be detected on the surface of P25 and TiO-4-180-4. The C 1s at approximate 284.5 eV may arise from adventitious carbon on the surface of samples.[27] For P25, the Ti $2p_{3/2}$ and Ti $2p_{1/2}$ peaks center at binding energies of 458.6 and 464.4 eV, respectively, which are characteristics of the Ti^{4+}–O bonds in TiO_2. However, these two peaks shift to lower binding energies of 458.2 and 464.0 eV for TiO-4-180-4 (Fig. 5a), which can be an indication of the existence of Ti^{3+} in the TiO-4-180-4. The binding energy of O 1s of TiO-4-180-4 shows a slight decrease compared with that of P25 (Fig. 5b). It has been reported that the shift of binding energies to lower region can be observed in the hydrogen reduced TiO_2 nanotube,[11] which is similar to our result. Consistent with Raman result, the XPS data also evidence that the formation of oxygen vacancies in TiO-4-180-4.

TiO_2 has been widely used as a support for various metal catalysts for selective catalytic hydrogenation,[6–8] oxidation[9,10] and electrochemical[11,12] reactions. There is a SMSI between TiO_2 and metal particles that induces unique catalytic performance. However, the SMSI was usually observed at high temperatures under reducing atmosphere, where TiO_2 was highly likely to be reduced.[28] Moreover, the specific surface area of TiO_{2-x} (TiO-4-180-4) is about 2.5 times as large as pristine P25. Therefore, it is very interesting to investigate the prepared TiO_{2-x} as catalyst support. There are growing research activities in employing hydrocarbons and N-heterocycles as liquid organic hydrogen carriers (LOHCs) in recent years because of their compatibleness with existing gasoline infrastructure facilitating the switch to hydrogen energy system.[29–31] Catalyst development for the hydrogenation and dehydrogenation of those LOHCs are of practical importance. In the context, the TiO_{2-x} supported Ru catalyst is prepared and tested for the hydrogenation of *N*-methylpyrrole, a commercially available LOHC with large annual global production.

As shown in Fig. 6a, uniformly distributed Ru on the pristine TiO_2 has a mean particle size of about 1.1 nm (Fig. S4†). The Ru supported on TiO_{2-x}, on the other hand, is hardly distinguishable by TEM (Fig. S5†), indicating even smaller particle size of Ru on TiO_{2-x}. Fortunately, the HAADF-STEM image evidences the presence of Ru particles (particle size < 1 nm, Fig. 6b), but the specific particle size is difficult to be calculated because of the ambiguous boundary of those particles. Considering the larger surface area and "rough" surface morphology of TiO_{2-x}, Ru may have better dispersion on TiO_{2-x}. Furthermore, oxygen vacancies or Ti^{3+} in TiO_{2-x} may also be helpful for anchoring metal particles and, thus, leading to better dispersion than that on pristine P25.[18]

Recent reports showed that the electron-rich transition metals could facilitate the hydrogenation of N-heterocycles.[32] The reduced state of TiO_{2-x} may also be favorable in electron transfer between support and Ru. As we expected, the XPS of Ru

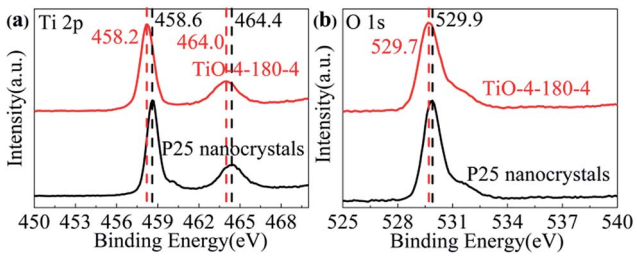

Fig. 5 (a) Ti 2p and (b) O 1s XPS of P25 nanocrystals and TiO-4-180-4.

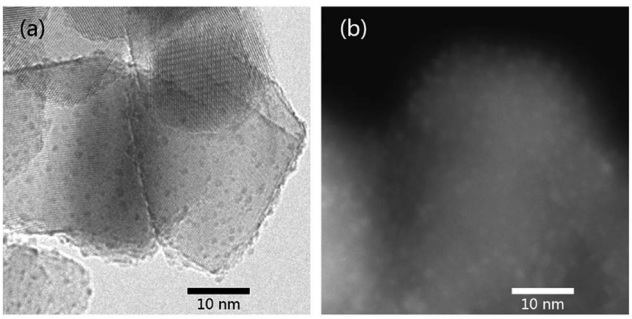

Fig. 6 (a) TEM image of 5 wt% Ru/TiO_2. (b) HAADF-STEM image of 5 wt% Ru/TiO_{2-x}.

$3d_{5/2}$ signal shows that the binding energy of Ru supported on TiO_{2-x} down shifts 0.5 eV as compared with that on TiO_2 (Fig. S6†), indicating an electron rich state of Ru on TiO_{2-x}, which also suggests a stronger interaction between support and metal particles.[33] Although Ru is known to catalyze the hydrogenation of *N*-methylpyrrole well,[34] the effect of catalyst support has not been well investigated. As shown in Fig. 7a, about 80% and 88% *N*-methylpyrrole can be hydrogenated to *N*-methylpyrrolidine in 60 min at 90 °C and 100 °C by using Ru/TiO_2 catalyst, respectively. Ru/TiO_{2-x}, on the other hand, shows superior catalytic performance compared to that of Ru/TiO_2, *i.e.*, about 91% and 95% *N*-methylpyrrole can be hydrogenated under the same condition. Furthermore, the initial hydrogenation rate on Ru/TiO_{2-x} at 100 °C is about twofold as that with Ru/TiO_2 (Table S1†), showing encouraging promotion effect of TiO_{2-x} as support. Calculated from the Arrhenius plots (Fig. 7b), the activation energies for the hydrogenation reaction are 50.9 kJ mol^{-1} and 50.0 kJ mol^{-1} for Ru/TiO_2 and Ru/TiO_{2-x}, respectively, suggesting similar hydrogenation mechanism for both catalysts. Therefore, the improved catalytic activity of Ru/TiO_{2-x} can be probably attributed to the better dispersion of Ru on the support, which is confirmed by the larger pre-exponential factor (*A*) as shown in Table S1.† We suggest that in addition to the larger specific surface area of TiO_{2-x} (113 m^2 g^{-1}), oxygen vacancies or Ti^{3+} in TiO_{2-x} may intensify the interaction between Ru particles and TiO_{2-x}, and therefore, enhancing the better dispersion of Ru particles by inhibiting Ru migration and agglomeration.[11] However, the strong interaction between TiO_{2-x} and metal particles is an interesting subject that needs to be further investigated and elucidated over reactions that are sensitive to the electronic state of transition metals.

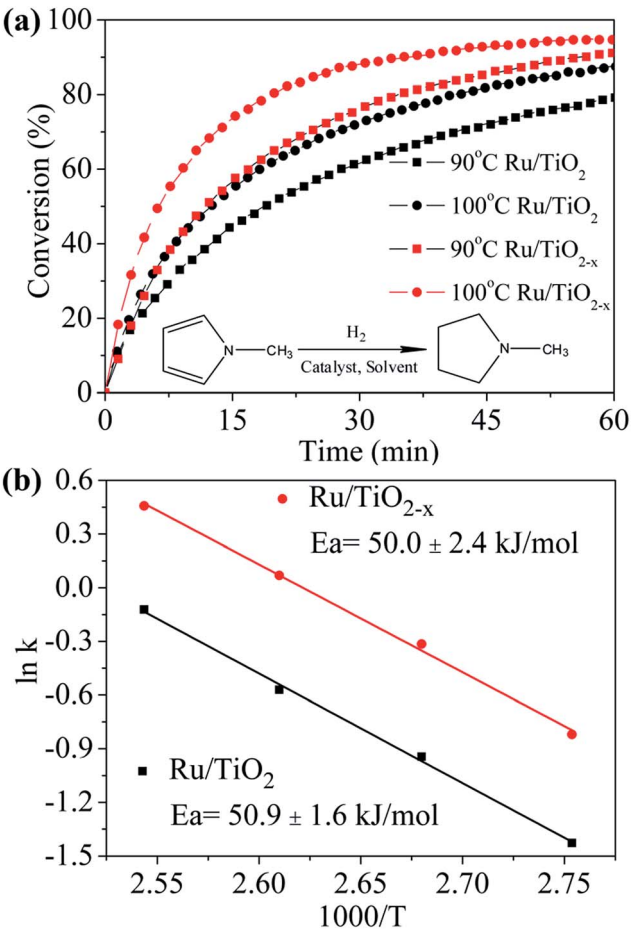

Fig. 7 (a) Hydrogenation of *N*-methylpyrrole with catalysts Ru/TiO_2 or Ru/TiO_{2-x} at 30 atm H_2 pressure, 90 °C and 100 °C, catalyst/substrate molar ratio is 1 : 100. (b) The Arrhenius plots in the temperature range of 363–393 K.

Conclusions

In summary, we have developed a room temperature solid reduction approach for the synthesis of nanosized TiO_{2-x} from TiO_2 crystals. A series of TiO_{2-x} with controllable reduction degree have been successfully synthesized by ball-milling of TiO_2 crystal with finely dispersed Na/NaCl powders. The obtained TiO_{2-x} with high surface area can be employed as an effective support for Ru particles and the Ru/TiO_{2-x} catalyst exhibited superior activity in catalytic hydrogenation of *N*-methylpyrrole, a commercial available heterocycle with large annual global production. We believe that this highly efficient room temperature reduction approach for the production of TiO_{2-x} offers a promising opportunity for the practical applications of TiO_{2-x} in different areas.

Acknowledgements

The authors would like to acknowledge financial support from the projects of National Natural Science Foundation of China (Grant No. U1232120, 21473181, 51671178 and 51472237), support from the Youth Innovation Promotion Association (CAS) and the CAS-Helmholtz Association Collaborative Funding.

Notes and references

1 A. Fujishima and K. Honda, *Nature*, 1972, **238**, 37–38.
2 J. H. Braun, A. Baidins and R. E. Marganski, *Prog. Org. Coat.*, 1992, **20**, 105–138.
3 R. Zallen and M. Moret, *Solid State Commun.*, 2006, **137**, 154–157.

4 A. L. Linsebigler, G. Lu and J. T. Yates Jr, *Chem. Rev.*, 1995, **95**, 735–758.
5 Z. Zhang and J. T. Yates Jr, *Chem. Rev.*, 2012, **112**, 5520–5551.
6 M. Vannice and R. Garten, *J. Catal.*, 1980, **66**, 242–247.
7 V. Kratky, M. Kralik, M. Mecarova, M. Stolcova, L. Zalibera and M. Hronec, *Appl. Catal., A*, 2002, **235**, 225–231.
8 X. Han, R. Zhou, G. Lai and X. Zheng, *Catal. Today*, 2004, **93**, 433–437.
9 S. Bonanni, K. Ait-Mansour, H. Brune and W. Harbich, *ACS Catal.*, 2011, **1**, 385–389.
10 A. Yoshida, Y. Mori, T. Ikeda, K. Azemoto and S. Naito, *Catal. Today*, 2013, **203**, 153–157.
11 C. Zhang, H. Yu, Y. Li, Y. Gao, Y. Zhao, W. Song, Z. Shao and B. Yi, *ChemSusChem*, 2013, **6**, 659–666.
12 L. Zhao, Z. B. Wang, J. Liu, J. J. Zhang, X. L. Sui, L. M. Zhang and D. M. Gu, *J. Power Sources*, 2015, **279**, 210–217.
13 X. B. Chen, L. Liu, P. Y. Yu and S. S. Mao, *Science*, 2011, **331**, 746–750.
14 Z. Wang, C. Yang, T. Lin, H. Yin, P. Chen, D. Wan, F. Xu, F. Huang, J. Lin, X. Xie and M. Jiang, *Adv. Funct. Mater.*, 2013, **23**, 5444–5450.
15 S. Tominaka, *Inorg. Chem.*, 2012, **51**, 10136–10140.
16 H. Tan, Z. Zhao, M. Niu, C. Mao, D. Cao, D. Cheng, P. Feng and Z. Sun, *Nanoscale*, 2014, **6**, 10216–10223.
17 X. Y. Pan, M. Q. Yang, X. Z. Fu, N. Zhang and Y. J. Xu, *Nanoscale*, 2013, **5**, 3601–3614.
18 M. Chen and D. Goodman, *Science*, 2004, **306**, 252–255.
19 S. Tauster, S. Fung and R. Garten, *J. Am. Chem. Soc.*, 1978, **100**, 170–175.
20 D. Goodman, *Catal. Lett.*, 2005, **99**, 1–4.
21 W. Chen, G. Wu, T. He, Z. Li, Z. Guo, H. Liu, Z. Huang and P. Chen, *Int. J. Hydrogen Energy*, 2016, **41**(34), 15371–15476.
22 F. Sirotti, M. De Santis and G. Rossi, *Phys. Rev. B: Condens. Matter Mater. Phys.*, 1993, **48**, 8299.
23 Z. Wang, C. Yang, T. Lin, H. Yin, P. Chen, D. Wan, F. Xu, F. Huang, J. Lin, X. Xie and M. Jiang, *Energy Environ. Sci.*, 2013, **6**, 3007–3014.
24 J. Zhang, M. Li, Z. Feng, J. Chen and C. Li, *J. Phys. Chem. B*, 2006, **110**, 927–935.
25 V. Likodimos, A. Chrysi, M. Calamiotou, C. Fernández-Rodríguez, J. Doña-Rodríguez, D. Dionysiou and P. Falaras, *Appl. Catal., B*, 2016, **192**, 242–252.
26 A. Li Bassi, D. Cattaneo, V. Russo, C. E. Bottani, E. Barborini, T. Mazza, P. Piseri, P. Milani, F. O. Ernst, K. Wegner and S. E. Pratsinis, *J. Appl. Phys.*, 2005, **98**, 074305.
27 C. Elmasides, D. I. Kondarides, W. Grunert and X. E. Verykios, *J. Phys. Chem. B*, 1999, **103**, 5227–5239.
28 G. L. Haller and D. E. Resasco, *Adv. Catal.*, 1989, **36**, 173–235.
29 A. C. Cooper, D. E. Fowler, A. R. Scott, A. H. Abdourazak, H. S. Cheng, L. D. Bagzis, F. C. Wilhelm, B. A. Toseland, K. M. Campbell and G. P. Pez, *Abstr. Pap. Am. Chem. S.*, 2005, **229**, U868.
30 R. H. Crabtree, *Energy Environ. Sci.*, 2008, **1**, 134–138.
31 T. He, Q. Pei and P. Chen, *J. Energy Chem.*, 2015, **24**, 587–594.
32 T. He, L. Liu, G. Wu and P. Chen, *J. Mater. Chem. A*, 2015, **3**, 16235–16241.
33 A. Lewera, L. Timperman, A. Roguska and N. Alonso-Vante, *J. Mater. Chem. C*, 2011, **115**, 20153–20159.
34 L. Hegedus, T. Mathe and A. Tungler, *Appl. Catal., A*, 1997, **161**, 283.